Chapter 7
Self-Organization of Network Structure in Coupled-Map Systems

Junji Ito and Kunihiko Kaneko

Abstract Coupled map models with variable connection weights between the units are studied. A generally observed feature in this type of model is the appearance of the units with massive outgoing connections. Such structure formation is the consequence of the feedback between unit and connection dynamics.

7.1 Introduction

Unveiling network structure is often important in studying biological and social systems. Universal topological properties of network structure have been found in a variety of natural and artificial networks [1–3]. Some of those properties such as scale-free or small-world structures have been shown to emerge from simple construction rules or by evolution of networks to achieve some function [4, 5]. Since the main interest in these early studies of complex networks was in the structure of networks, the dynamics of the constituent units were largely ignored.

Recently, more and more studies on complex networks have taken into account the activity of nodes and/or the flow through links, since they are often primary determinants of network growth or structure formation. For example, the relationship between abundances of chemicals on nodes in a chemical-reaction network has been studied from the viewpoint of the optimization of metabolic flow through the network [6, 7]. In these studies, each unit (i.e., chemical concentration) on a node is in a stationary state and therefore the interplay between the dynamics of the units and the network structure is not considered. This aspect is sought in another line of studies where behaviors of coupled dynamical systems in a network of units with non-trivial dynamics are extensively investigated. Some of those studies searched for the synchronization condition for oscillatory elements in a network and examined how it depends on network topology [5, 8–10], while others focused on dynamical systems of chaotic elements on a network interacting through links, which show

J. Ito (✉)
Theoretical Neuroscience Group, RIKEN Brain Science Institute, 2-1 Hirosawa, Wako, Saitama 351-0198, Japan
e-mail: j-ito@brain.riken.jp

T. Gross, H. Sayama (eds.), *Adaptive Networks,* Understanding Complex Systems,
DOI 10.1007/978-3-642-01284-6_7,

synchronization, clustering, and chaotic itinerancy [11–15]. In these studies, though the units on the network showed rich dynamics, the network structure itself was not dynamic: once initially given, it did not change in time. Following these previous studies, the next step should be to seek common principles in systems with an interplay between the network structure formation and dynamical systems on the network [16–21].

Adaptive network is the term given to the types of network whose structure varies depending on the dynamics of the units on the nodes [22]. The aim of the present study is to discover the generic features in the dynamics and the structure of adaptive networks. We adopt the system of coupled maps with variable connection weights as our tool to explore a class of models for adaptive networks, as coupled map dynamics have been thoroughly investigated for cases with various forms of fixed regular couplings [23–27]. We mainly focus on how non-trivial dynamic structure emerges from homogeneous populations of units and connections, and try to extract the underlying mechanisms of such structure formation.

We review three types of coupled map models, following our earlier studies [16–18]: the first one is coupled logistic maps, the second one is coupled circle maps, and the last one is coupled circle maps with external input. For all these three models, coupling strengths between nodes change according to the correlation between the values on the nodes. For the first model, an exhaustive analysis of unit and connection dynamics is given in Sect. 7.2. To avoid redundant description on similar behaviors in different models, only the characteristic behaviors specific to the latter two models are described in Sects. 7.3 and 7.4. The last section is a summary and discussion on our findings.

7.2 Adaptive Network of Logistic-Map Units

Throughout the present review we discuss a system of coupled maps on a network. Each node in the network is assigned with map dynamics which depend on the instantaneous state of the node as well as on those of the other nodes that are linked to it. This sort of dynamical system is known as *coupled maps* and has been extensively studied over decades. In particular, coupled map lattices with nearest neighbor couplings on a regular lattice [23, 24] and globally coupled maps (GCM) with all-to-all coupling of equal weight [25] are two standard models. Here we adopt the coupled map approach, but instead of fixed global or nearest-neighbor couplings a time-varying connection weight is introduced in our models.

In this section, we consider the model of coupled logistic maps. Logistic map is a nonlinear map from x_n to x_{n+1} with one parameter a representing its nonlinearity, defined as:

$$x_{n+1} = ax_n(1 - x_n). \tag{7.1}$$

Successive application of this mapping yields, depending on the value of the parameter a, oscillatory dynamics with arbitrary period as well as chaotic dynamics.

Owing to this variety in dynamics, one network of logistic-map units can represent a wide range of networks with various kinds of unit dynamics. For this reason, this type of network is of primary and special interest in our study.

7.2.1 Model Formulation

Our coupled map model is defined as follows. Suppose we have a network of N units, each of which has its own time-dependent internal state. Let x_n^i denote the state variable of the i-th unit ($1 \leq i \leq N$) at the n-th time step. Connectivity between these units is given by the connection matrix w_n^{ij} which represents the weight (or strength) of the connection from unit j to unit i at the n-th time step. To introduce dynamics to the network, we install the following two functions into our model. One is the function f that defines the mapping from x_n^i to x_{n+1}^i, in other words, the dynamics of the units. The other is the function g that represents the rule of connection change. For simplicity, we assume that the range of g is between 0 and 1, and g depends only on the two state variables of the units at the both ends of the connection. With this setup, our model is described by the following set of equations:

$$x_{n+1}^i = (1-c) f(x_n^i) + c \sum_j w_n^{ij} f(x_n^j), \tag{7.2}$$

$$w_{n+1}^{ij} = \frac{[1 + \delta g(x_n^i, x_n^j)] w_n^{ij}}{\sum_j [1 + \delta g(x_n^i, x_n^j)] w_n^{ij}}, \tag{7.3}$$

where c ($0 \leq c \leq 1$) is the parameter that represents the strength of the interaction between units and δ ($0 \leq \delta \leq 1$) is the parameter that represents the degree of plasticity of connections. The normalization of incoming connection weights in Eq. (7.3) is introduced in order to avoid the divergence of connection weights in the case where the steady state of unit dynamics satisfies strengthening condition of the connection change, which could lead to endless growing of the connection weights. This normalization also imposes competition among incoming connections of a unit. When $\delta = 0$, this model reduces to the standard GCM.

By choosing appropriate functions for f and g, Eqs. (7.2) and (7.3) can model various types of adaptive networks. This choice would depend on the purpose of modeling. For example, connection dynamics that strengthen the connections between units in different dynamical states would lead to global synchronization of the whole system. This type of rewiring rule is introduced by Chen and Kurth to a coupled phase oscillator model and described in detail in the subsequent chapter. In this study, however, we focus on the opposite type of connection dynamics, i.e., "Hebbian" type dynamics, which is characterized by the strengthening of connections between units in a similar state. This type of dynamics is called Hebbian because it can be considered as a natural extension of the Hebb rule, which is widely used as a synaptic update rule in neural network studies and considered as the

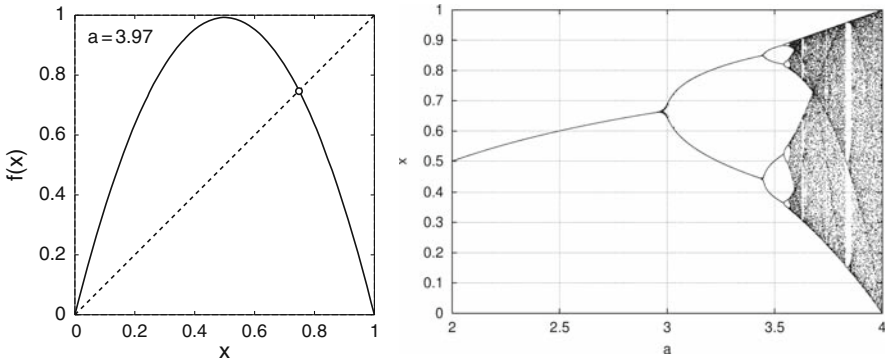

Fig. 7.1 The logistic map and its bifurcation diagram. (*Left*) The mapping function $f(x) = ax(1 - x)$; $a = 3.97$. The *open circle* in the graph represents the unstable fixed point of the dynamics generated by this map. (*Right*) The bifurcation diagram of logistic map. Asymptotic values of x are plotted for each value of the parameter a. This map generates chaotic dynamics for values of a larger than about 3.57

fundamental principle of structure formation in neural networks, to systems with continuous state variables. The function that we use in practice for the connection dynamics in our simulations is $g(x^i, x^j) = 1 - 2|x^i - x^j|$, but any other function which monotonically decreases with the difference between its two arguments gives essentially identical results. For unit dynamics, as mentioned above, we adopt the logistic map: $f(x^i) = ax^i(1 - x^i)$. Figure 7.1 shows the graph of this mapping function and how the unit dynamics depend on the value of the parameter a.

To this end, our model possesses three parameters: a for the nonlinearity of unit dynamics, c for the strength of interaction between units, and δ for the plasticity of connection. In this section, δ is set to 0.1, though a wide range of δ values give similar results [17].

In the following, we study the dynamics of the networks described by Eqs. (7.2) and (7.3) using numerical simulations. In most of the simulations, we use the following initial condition. First, the initial value of self-connection w_0^{ii} is set to 0 for all i. This assures that the self-connections (besides the term $(1 - c) f(x_n^i)$) are 0 at any time step n. Second, all the remaining connection weights are set to be identical. This means that, at the initial step, every unit in the system uniformly connects to all the other units. Due to the normalization of incoming connections, the initial connection weight is determined to be $1/(N - 1)$. Finally, x_0^i are randomly chosen from the uniform distribution between 0 and 1.

7.2.2 Unit Dynamics

We start our analysis from studying the dependence of unit dynamics on the values of the parameters a and c. It is known that the dynamics of coupled map systems are characterized by the formation of synchronized clusters of units. In Fig. 7.2,

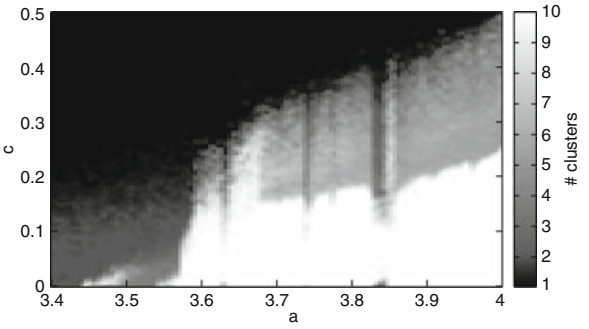

Fig. 7.2 The number of clusters plotted against the parameters a and c, obtained from the numerical simulations of our model composed of 10 units. The number of clusters is counted after 5,000 steps of transient period and averaged over 100 simulations starting from random initial conditions

the number of clusters observed in our model is plotted against the parameters a and c. Basically, the number of clusters increases as a gets larger or c gets smaller, which is consistent with the previous studies of GCM [25] where the connection weights are constant over elements and time. A novel dynamical feature induced by the introduction of connection change is the appearance of a large regime of $N/2$-cluster state in the (a, c)-space. In this state, every unit forms a pair with another unit and the state variables of the units in a pair are synchronized, resulting in $N/2$ clusters in the system. Destabilization of this pair (by increase of a or decrease of c) immediately results in the total absence of synchronized clusters, because all the units in our model have the same set of parameter values, and therefore, once a pair is destabilized, so are all the other pairs as well. This means that there is hardly any set of parameter values that allows an intermediate number of clusters between $N/2$ and N.

In the following, we give a more detailed description for the three representative states of unit dynamics observed in our model.

Synchronized state: For small a and large c values, all the units in the system are synchronized. The dynamics of the units are either periodic or chaotic, depending on the value of a (Fig. 7.3a). The connection weights do not change in this state, because in our model, connection dynamics are driven by the difference between the state variables, and all the state variables have an identical value in the synchronized state. Due to this lack of connection dynamics, the system is essentially identical to the standard GCM. The stability of the synchronized state in the standard GCM can be estimated using the tangential Lyapunov exponent, or split exponent [25], defined as follows for our model:

$$\lambda_{\mathrm{spl}}(a, c) = \ln\left(1 - \frac{N}{N-1}c\right) + \lambda_0(a), \tag{7.4}$$

where λ_0 represents the Lyapnov exponent of, in our case, the logistic map with parameter value a. With this quantity, the stability condition for the synchronized state is written as $\lambda_{\mathrm{spl}}(a, c) < 0$, and hence the boundary of the region (in (a, c)-space) where a synchronized state is allowed is given by:

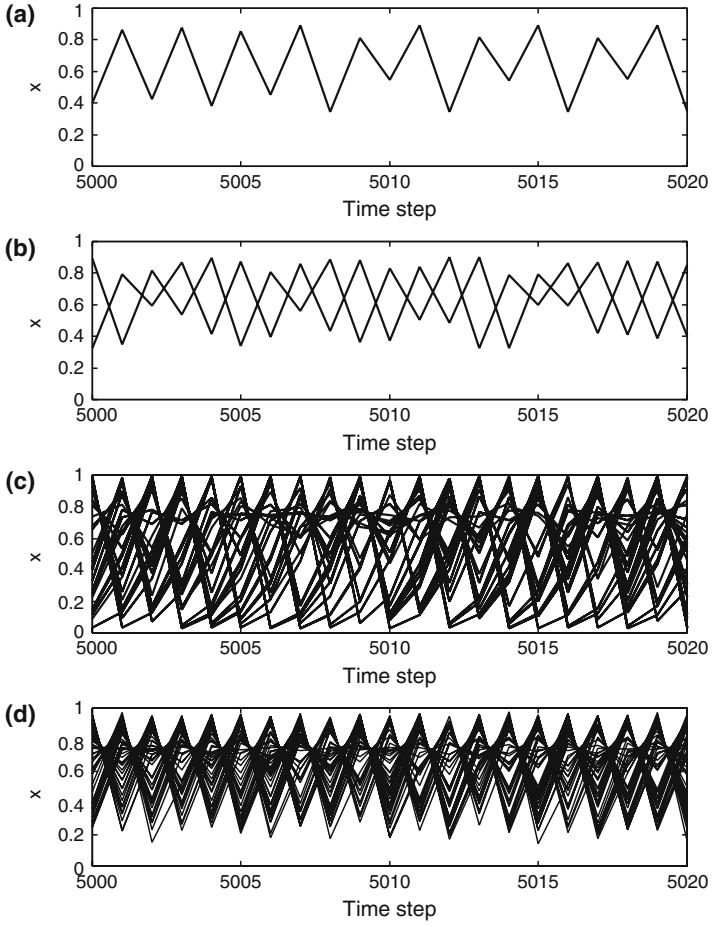

Fig. 7.3 Time series of x_n^i $(1 \leq i \leq N, N = 50)$. Traces for all state variables are superimposed. (**a**) coherent state. $a = 3.6, c = 0.3$. (**b**) ordered state with two clusters. $a = 3.6, c = 0.2$. (**c**) ordered state with N/2 clusters. $a = 3.97, c = 0.3$. (**d**) desynchronized state. $a = 3.97, c = 0.125$

$$\ln\left(1 - \frac{N}{N-1}c\right) + \lambda_0(a) = 0. \tag{7.5}$$

Desynchronized state: For large a and small c values, unit dynamics are not synchronized between any pair of units. Each unit shows chaotic dynamics (Fig. 7.3d). Due to the difference between the state variables, connection weights show temporal change, which can lead to self-organization of network structure. The interaction between unit and connection dynamics will be discussed later in detail.

Clustered state: For intermediate values of a and c, units spontaneously form clusters, within which units oscillate synchronously. The dynamics of the units are either periodic or chaotic, depending on the value of a (Fig. 7.3b, c). The con-

nection weights between the units in the same cluster do not vary in time, while the connection between units in different clusters can have temporal change. The number of the clusters is 2 near the boundary with the synchronized state region. As a gets larger or c gets smaller, the number increases to reach the maximum number $N/2$ at the boundary against the desynchronized state. As mentioned above, in an $N/2$-cluster state, every unit forms a pair and the two units in a pair synchronize to each other. The stability of the $N/2$-cluster state can be evaluated again with the split exponent according to the following argument. Due to the increase in connection strength between the units forming a pair (and the normalization of incoming connections), the connection between the units in different pairs vanishes. In this state, a unit in a pair interacts only with its partner and therefore the system can be regarded as a collection of GCM of 2 units. Hence, the estimation of the stability of this state is reduced to that of a small GCM system. The split exponent of GCM of 2 units is obtained by substituting 2 to N in Eq. (7.4), resulting in $\lambda_{\rm spl}(a, c) = \ln(1 - 2c) + \lambda_0(a)$. Thus, the boundary between the region of the $N/2$-cluster state and that of the desynchronized state is given by:

$$\ln(1 - 2c) + \lambda_0(a) = 0. \tag{7.6}$$

According to Eqs. (7.5) and (7.6), we define in the (a, c)-space the following three phases, named after those in GCM system [25]: (I) *coherent phase*, which is above Eq. (7.5), (II) *ordered phase*, which is between Eqs. (7.5) and (7.6), and (III) *desynchronized phase*, which is below Eq. (7.6).

7.2.3 Connection Dynamics

We proceed to study connection dynamics, which are largely influenced by the unit dynamics discussed above. It is intuitively expected that connection weights would be kept constant in the coherent and ordered phases and that they would show active dynamics in the desynchronized phase. To confirm this in a quantitative manner, we define a measure of the network activity, which represents the intensity of temporal change in connection weights, as follows:

$$A = \frac{1}{(N-1)^2} \sum_{i \neq j} \langle |w_n^{ij} - w_{n-1}^{ij}| \rangle, \tag{7.7}$$

where $\langle \cdot \rangle$ stands for temporal average taken after an appropriate transient period. This is the connection change in one time step averaged over time and over connections. Figure 7.4(top) is the plot of A against the parameters a and c. As expected, It can be seen that A is zero in the coherent and the ordered phases and that finite values of A are observed only within the desynchronized phase. An interesting point is that there are regions in the desynchronized phase where A takes extremely small

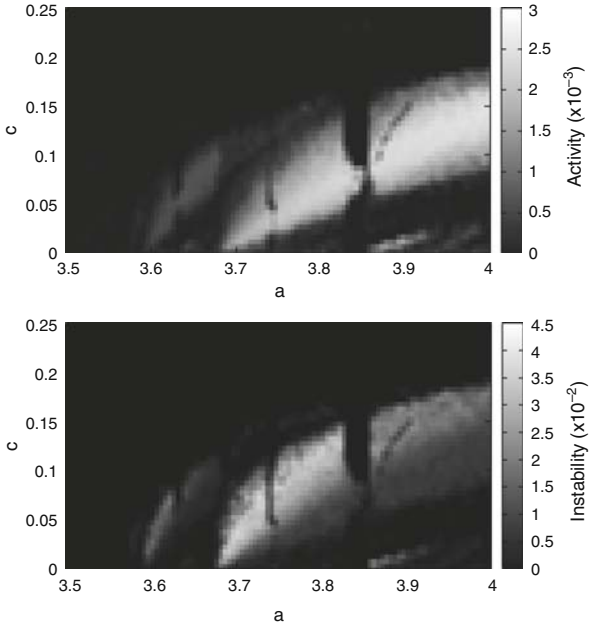

Fig. 7.4 Plot of the activity A (*top panel*) and the instability I (*bottom panel*) of the network against the parameters a and c, obtained from the numerical simulation of our model composed of 10 units. The values of A and I are calculated from w_n^{ij} values during the 1,000 steps after 100,000 steps of transient period. The network activity A represents the intensity of connection change and the network instability I represents the fragility of network structure. See the main text for their definitions

values, and that the region of large A values forms a complex structure in (a,c)-space.

Vanishing values of A reflect diminishing connection change, which means the appearance of long-lasting structure in the network. From Fig. 7.4(top), it is expected that such network structures are present in the coherent and the ordered phases, and also in a part of the desynchronized phase where A shows extremely small values. On the other hand, large values of A reflect active connection dynamics. Under such situation, it seems impossible for a stable structure to survive in the network. However, there is a possibility that the change in connection weights is due to fluctuations around some fixed values, which are kept stable over time. In such a case, the network activity A takes a non-zero value but some stable structure is preserved in the network. To check for this possibility, we define a measure for the instability of network structure using the temporal variance of connection weight around its mean as follows:

$$I = \frac{1}{(N-1)^2} \sum_{i \neq j} \left(\langle {w_n^{ij}}^2 \rangle - \langle w_n^{ij} \rangle^2 \right), \tag{7.8}$$

where $\langle \cdot \rangle$ is the temporal average as in Eq. (7.7). Large I values reflect that connection weights have large fluctuations and are not fixed in time so that the network structure is unstable. Figure 7.4(bottom) is the plot of I against the parameters a and c. By definition, $I = 0$ in the area where $A = 0$, which corresponds to the trivial fact that if there is no connection change, network structure is maximally stable. An

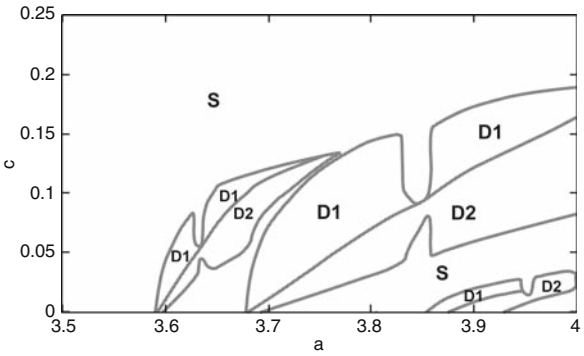

Fig. 7.5 A rough phase diagram illustrating the regions in the desynchronized phase. Letters in the panel stand for static region (S), where static networks are observed, dynamic region I (D1), where dynamic and unstable networks are observed, and dynamic region II (D2), where dynamic and stable networks are observed. See the main text for the definition of the regions

interesting observation is that the high activity region in Fig. 7.4(top) seems to be separated into two subregions; one with large I values and the other with moderate, namely ~ 0.01, I values. For example, at $a = 3.8$, the intervals $0.03 < c < 0.07$ and $0.07 < c < 0.13$ seem to belong to the moderate I and the large I subregions, respectively. This implies the possibility that dynamic but structured networks are allowed to exist in certain parts of the desynchronized phase.

Based on these observations, we separate the desynchronized phase into three regions (Fig. 7.5): (i) static region, characterized by extremely small A values, (ii) dynamic region I, characterized by large A values and large I values, and (iii) dynamic region II, characterized by large A values and moderate I values.

7.2.4 Network Structure

As mentioned above, in the beginning of the numerical simulations, connection in the network is uniform and all-to-all. From this initial condition, the system develops to various kinds of structured network, depending on the type of unit dynamics. Here we run through the phases and the regions and see what type of network structure is formed in each of the phases (regions) by examining the connection matrix w^{ij}.

(I) *Coherent phase*: A snapshot of the connection matrix in this phase is shown in Fig. 7.6a. In this phase, all-to-all connection is preserved as in the initial state. Connection weights are, however, distributed around the initial values due to the connection change during the transient to the asymptotic state, i.e., synchrony among all the units. Once the synchronization is achieved, no further connection change occurs.

(II) *Ordered phase*: Snapshots of the connection matrix in this phase are shown in Fig. 7.6b, c. In this phase, network structure depends on the clustering of units. Once the clusters are formed, connections within a cluster are strengthened and ones across clusters are weakened, resulting in vanishing connection weights between clusters. In the case of a 2-cluster state, the network separates into two almost independent sub-networks, within which units are connected in all-to-all fashion

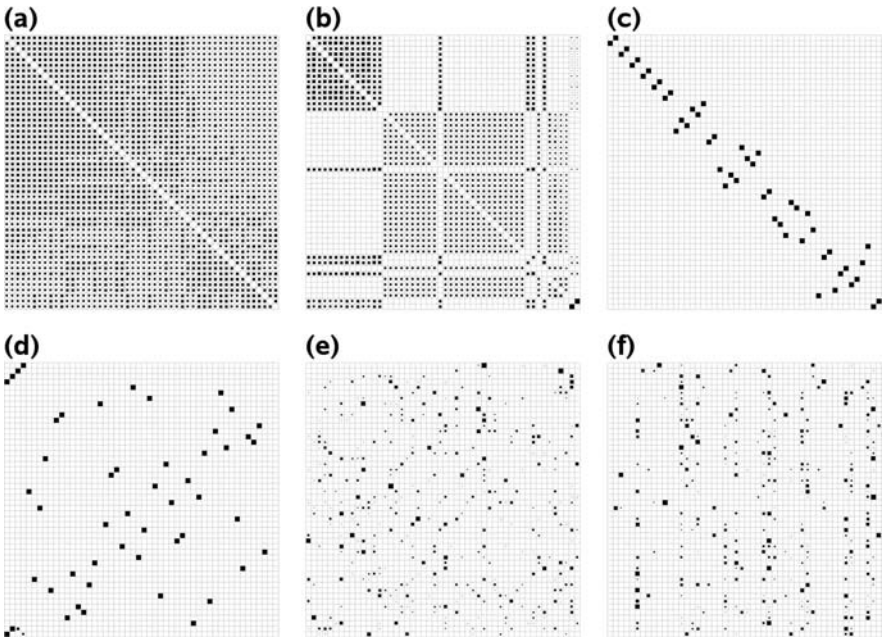

Fig. 7.6 Snapshots of the connection matrix w^{ij} in different phases/regions. The value of w^{ij} is indicated by the size of the filled square at the i-th row and the j-th column. (**a**) Coherent phase. $a = 3.6, c = 0.3$. (**b**) Ordered state with two clusters. $a = 3.6, c = 0.2$. (**c**) Ordered state with N/2 clusters. $a = 3.97, c = 0.3$. (**d**) Static region in desynchronized state. $a = 3.97, c = 0.2$ (**e**) Dynamic region I in desynchronized state. $a = 3.97, c = 0.15$. (**f**) Dynamic region II in desynchronized state. $a = 3.97, c = 0.125$

(Fig. 7.6b). As mentioned above, the maximum number of clusters is $N/2$. In an $N/2$-cluster state, units form pairs and have connections only within the pairs (Fig. 7.6c).

(III) *Desynchronized phase*: This phase is separated into three regions.

(i) *Static region*: A snapshot of the connection matrix in this region is shown in Fig. 7.6d. This region is characterized by low network activity A. In this region, most units make pairs and each unit is connected only with its partner. Although their connection strengths hardly change over time, decomposition and recomposition of pairs occasionally occurs. Besides those units forming pairs, a few units that do not form pairs remain. Their connection weights show rapid changes over time. The dynamics of units forming a pair are not synchronized, but highly correlated, while there is almost no correlation between units that belong to different pairs.

(ii) *Dynamic region I*: A snapshot of the connection matrix in this region is shown in Fig. 7.6e. This region is characterized by high network activity A and high structural instability I. There is no synchronization between any two units, and the correlation between units is very weak for any pair of units. Due to these disordered unit dynamics, connection weights change intensely, and the network structure seems to be random.

(iii) *Dynamic region II*: A snapshot of the connection matrix in this region is shown in Fig. 7.6f. This region is characterized by high network activity A and moderate structural instability I. Similarly to the dynamic region I, there is neither synchronization nor a significant correlation between any two units. Here the network seems to possess a certain structure which is characterized by the concentration of outgoing connection weights to a small fraction of units, although the connection weights change as intensely as in dynamic region I.

In the rest of this section, we focus on the dynamic networks observed in the desynchronized phase and study their structure and dynamics in detail.

7.2.5 Dynamic Networks in the Desynchronized Phase

In this part, we focus on the networks observed in dynamic regions I and II, and study the difference between the two networks in both structural and dynamical aspects. Here, we use the parameter values $(a, c) = (3.97, 0.15)$ for dynamic region I and $(a, c) = (3.97, 0.125)$ for dynamic region II.

7.2.5.1 Network Structure and Its Stability

To compare the structural properties of the networks in a quantitative manner, we characterize their structure from the values of w^{ij}. First, we look at the distribution of w^{ij} values. Figure 7.7a shows the distributions calculated for the networks from dynamic region I and II. Though larger values are observed slightly more often in dynamic region II, the distribution of w_{ij} values has quite similar shape in both of the regions, meaning that the apparent difference in the network structure seen in Fig. 7.6d, f is not due to the difference in the connection weights but based solely on

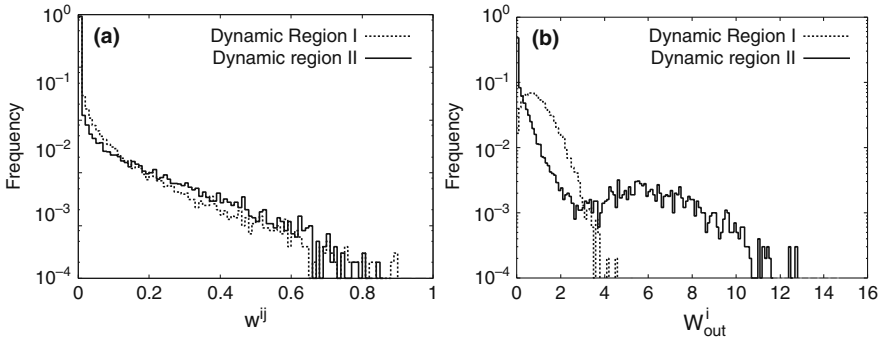

Fig. 7.7 Distributions of the values of connection matrix w^{ij} and those of the total weight of outgoing connection weights ${W_{\text{out}}}^i$ in dynamic region I and II. (**a**) Distribution of w^{ij} in dynamic region I and II. Values of w^{ij} at the 500,000th step are collected from 10 simulations. (**b**) Distribution of ${W_{\text{out}}}^i$ in dynamic region I and II. Values of ${W_{\text{out}}}^i$ at the 500,000th step are collected from 100 simulations

the manner in which they connect the units. Next, to assess how the distribution of the connections differs across units, we look at the distribution of the sum of outgoing connection weights $W_{\text{out}}{}_n^i = \sum_j w_n^{ji}$. Figure 7.7b shows the distribution of $W_{\text{out}}{}^i$ values for the networks from dynamic region I and II. The distributions are clearly different. In dynamic region I, the distribution is unimodal with the peak at around 0.7 and shows exponential (or even faster) decay for large values. In dynamic region II, there are two peaks in the distribution: the main peak is at 0 and the distribution shows exponential (or slower) decay, while the other peak is at around 6, suggesting the existence of a small group of units that have very large $W_{\text{out}}{}^i$ values.

As these distributions are calculated from the instantaneous values of w^{ij}, they tell us nothing about how the network changes its structure in time. To illustrate the temporal evolution of network structure, time series of $W_{\text{out}}{}^i$ for the network in dynamic region II is plotted for all i in Fig. 7.8. In this plot, units are separated into two groups according to the $W_{\text{out}}{}^i$ value at the 10^7th step: units that have $W_{\text{out}}{}^i$ values larger than 2 are plotted in gray, and the others are plotted in black. By retrospectively tracing the $W_{\text{out}}{}^i$ values of each of the groups, it is confirmed that the separation of units into the two groups is already evident at a very early stage of the temporal evolution, namely at the 2.0×10^6th step or even earlier. The moderate value of the network instability I in dynamic region II reflects this stable separation of units into large and small $W_{\text{out}}{}^i$ groups.

To assess this separation in a quantitative manner, we define an autocorrelation function regarding the separation of units in the following way. First, as a preparation step, we define a membership function μ as follows:

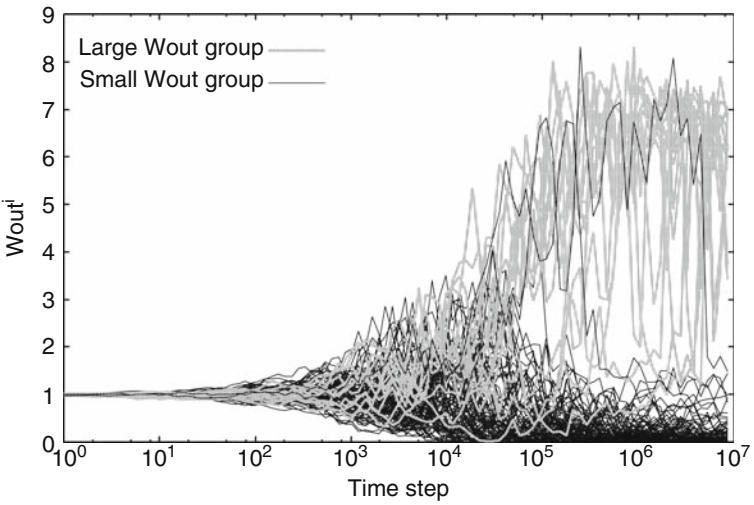

Fig. 7.8 Temporal evolution of $W_{\text{out}}{}^i$ in a network observed in dynamic region II. The values of $W_{\text{out}}{}^i$ at each 10^4 steps are plotted. Traces for all units are superimposed. The colors indicate the value of $W_{\text{out}}{}^i$ at the 10^7th step: units with a $W_{\text{out}}{}^i$ value larger than 2 are plotted in *gray*, and the others in *black*. $N = 100$

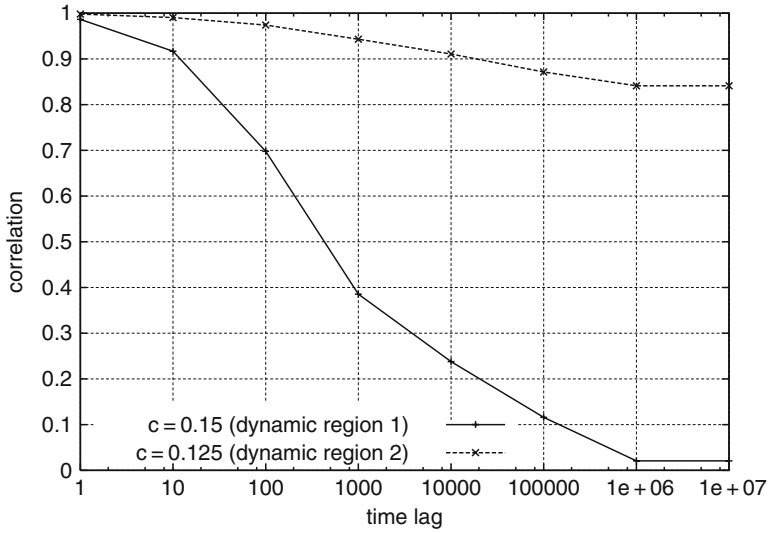

Fig. 7.9 The temporal autocorrelation $C_{\text{sep}}(\tau_l)$ regarding the separation of units, plotted for different values of τ_l. See the main text for the definition of $C_{\text{sep}}(\tau_l)$

$$\mu({W_{\text{out}}}^i) = \begin{cases} 1 & ({W_{\text{out}}}^i \geq 1.0) \\ -1 & ({W_{\text{out}}}^i < 1.0) \end{cases} \tag{7.9}$$

This function indicates whether unit i belongs to the large or small ${W_{\text{out}}}^i$ group. The threshold value 1.0 used here is the average of the total outgoing connection weight of a unit. With this function, we define the temporal autocorrelation C_{sep} regarding the separation as follows:

$$C_{\text{sep}}(\tau_l) = \frac{1}{N} \sum_i \langle \mu({W_{\text{out}}}_n^i) \mu({W_{\text{out}}}_{n+\tau_l}^i) \rangle, \tag{7.10}$$

where $\langle \cdot \rangle$ is the temporal average as in Eq. (7.7). We measure the stability of the separation by computing the decay of C_{sep} with the increase of τ_l. A plot of C_{sep} for different values of τ_l is shown in Fig. 7.9. In dynamic region II, the correlation decays very slowly and remains as large as 0.84 even for a lag of 10^7 steps, while in dynamic region I, the correlation decays to almost zero within 10^6 steps. This shows that the separation of the units into the high and low ${W_{\text{out}}}^i$ groups is highly stable in dynamic region II, while the separation is unstable, or never appears, in dynamic region I.

7.2.5.2 Mechanism of Structure Formation

In this section, we study the relationship between unit dynamics and the change in network structure to reveal the mechanism of the structure formation.

In the dynamic regions, each unit is connected to many other units in a complex manner. To gain an intuition about how the units interact with each other during the course of structure formation, we examine the dynamics of the correlations between a given unit and the others, by calculating the correlations during a short time period, namely ten steps, and observing their temporal evolution.

In Fig. 7.10 (bottom), the time series of x^1 in a simulation of a network in dynamic region I and the correlations between x^1 and the other x^is are shown. The temporal dynamics of the correlations have the following characteristics: (1) strong positive or negative correlation lasts for a certain number of steps, followed by a short period with weak correlation; (2) after this period, the sign of the correlation reverses in most cases. The unit dynamics in dynamic region II also show the same characteristics, though the interval between the succeeding weak correlation periods is much longer than in dynamic region I.

The period of weak correlation sometimes appears simultaneously for all units. Note that this simultaneous appearance of the weak correlation period coincides with the approach of x^1 to the unstable fixed point ($x = 0.748\ldots$), which is typically accompanied by a reduced oscillation amplitude (Fig. 7.10 (top)). The dynamics of the logistic map here is dominated by the oscillation around the unstable fixed point: the state variables take values larger or smaller than this fixed point alternately. According to the phase of this oscillation, units are naturally separated

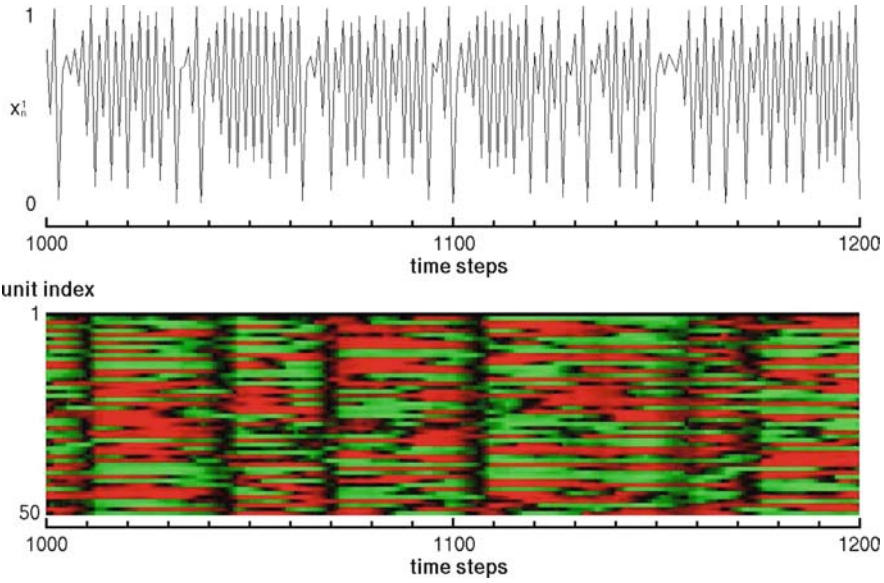

Fig. 7.10 Time series of x^1 in a simulation (*top*) and temporal evolution of the instantaneous correlations (for 10 steps) between unit 1 and the others (*bottom*), obtained from a simulation of the network in dynamic region I. The correlations are plotted in a color scale, where *green or red* represents positive or negative correlation, respectively, and the brightness of the colors indicates the magnitude of correlation

into two groups: when the units of one group take large values, the others take small values, and vice versa. This separation is not fixed over time. Indeed, each unit sometimes fails to jump over the fixed point, which reverses the phase of the oscillation. As a unit moves across the groups, the sign of the correlations to the other units changes at once, because the phase relationships to the other units are flipped to the opposite simultaneously. The periods with weak correlation seen in Fig. 7.10 correspond to the occurrences of this movement of units from one group to the other. We call this motion across the groups trans-group hopping (TGH). TGH is closely related to the temporal change in correlations between units. Hence, the dynamics of TGH are expected to have a strong influence on the formation of network structures.

To uncover the interaction between the dynamics of TGH and structure formation in the network, we study how the interval between two succeeding TGHs is related to the process of the network structure formation. The TGH interval is measured with the following method. After a transient period of τ_f steps, we fix the connection weights and only allow for the evolution of the state variables. Then we measure the TGH intervals for a certain time period and compute the average interval, separately for each of the units. In this way we estimate the expected TGH interval at an arbitrary stage in the process of the structure formation.

In Fig. 7.11, we plot the average TGH intervals of units against ${W_{\text{out}}}^i$ for several different values of τ_f, i.e., at several different stages of network structure formation. Initially, TGH intervals are almost same for all units (Fig. 7.11a). Then, the intervals

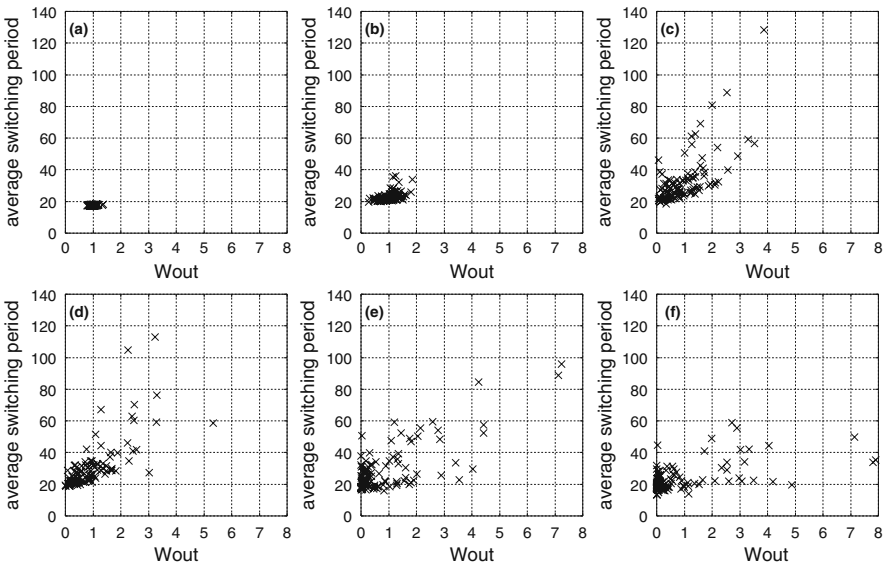

Fig. 7.11 Average TGH interval of units plotted against ${W_{\text{out}}}^i$ values. The intervals are calculated with connection weights fixed after τ_f steps of connection dynamics. (**a**) $\tau_f = 100$. (**b**) $\tau_f = 1,000$. (**c**) $\tau_f = 5,000$. (**d**) $\tau_f = 10,000$. (**e**) $\tau_f = 50,000$. (**f**) $\tau_f = 100,000$

become diverse among units (Figs. 7.11b–d). During these stages, TGH intervals are positively correlated to ${W_{\text{out}}}^i$, meaning that a unit with a larger ${W_{\text{out}}}^i$ value has a long TGH interval. Finally, at later stages, the correlation between TGH interval and ${W_{\text{out}}}^i$ gets weaker (Figs. 7.11e, f), but the separation of units into the large and small ${W_{\text{out}}}^i$ groups remains. This observation tells us that during the process of network structure formation, variety in the values of ${W_{\text{out}}}^i$ among units is positively reflected in TGH interval of the units: a unit with a large ${W_{\text{out}}}^i$ value has a long TGH interval (or a low TGH rate).

Next, we consider the opposite relationship, i.e., the influence of unit dynamics on the formation of the network structure. Here we study how the TGH interval is related to the correlation between units, which is directly reflected in the strengthening or weakening of connections. We measure the average correlation C^i of unit i to all the other units, defined as follows:

$$C^i = \frac{1}{N-1} \sum_{j \neq i} \frac{|\langle x_n^i x_n^j \rangle - \langle x_n^i \rangle \langle x_n^j \rangle|}{\sqrt{\langle {x_n^i}^2 \rangle - \langle x_n^i \rangle^2} \sqrt{\langle {x_n^j}^2 \rangle - \langle x_n^j \rangle^2}}. \tag{7.11}$$

In Fig. 7.12, the average correlation C^i, calculated in the network structure at the 10,000th step, is plotted against the average interval of TGH. A simple relationship can be recognized between C^i and TGH interval. A unit with a longer TGH interval has a stronger average correlation. Since C^i gives a measure of the degree of the increase in connections between unit i and the other units, this result suggests that a unit with a longer TGH interval is more likely to strengthen its connections.

Combining the influences from unit to connection dynamics and the other way around, the mechanism of network structure formation can now be understood as follows. A unit with a lower TGH rate grows its connections more rapidly than the others, and a unit with stronger outgoing connections decreases its rate of TGH. This mutual enhancement amplifies the difference in the outgoing connection weights

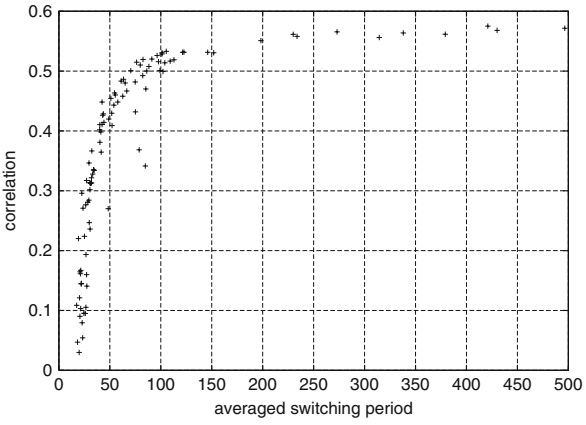

Fig. 7.12 The average correlation C^i of units plotted against the average TGH interval. The correlations are calculated with connection weights fixed after 10,000 steps of connection dynamics. See the main text for the definition of C^i

among units. The consequence of this amplification is the separation of units into the large and the small ${W_{\text{out}}}^i$ groups observed in dynamic region II.

7.3 Adaptive Network of Bursting Units

In the dynamics of the logistic map, oscillation around the unstable fixed point is dominant. Indeed, the mechanism of the network structure formation revealed in the previous section is closely related to this type of oscillatory dynamics. Hence, in order to infer the generality of such self-organization of network structure, it is necessary to check whether a similar kind of structure formation is observed in models with other unit dynamics. For this purpose, in this section, we consider a coupled-map model which is composed of circle-map units.

7.3.1 Model Formulation

The circle map, which is obtained by the discretization of a nonlinear phase oscillator, is defined as follows:

$$x_{n+1} = x_n + \omega + \frac{K}{2\pi} \sin 2\pi x_n \bmod 1, \tag{7.12}$$

where ω is the characteristic angular velocity and K represents the nonlinearity of the map. As the parameter K gets larger, this map yields more complex dynamics and finally gains the property of excitability, characterized by highly nonlinear responses to external perturbations due to the closely located stable and unstable fixed points, as shown in Fig. 7.13. Here we use the parameter values corresponding to Fig. 7.13, so that each unit is an excitable system from a stable fixed point. We

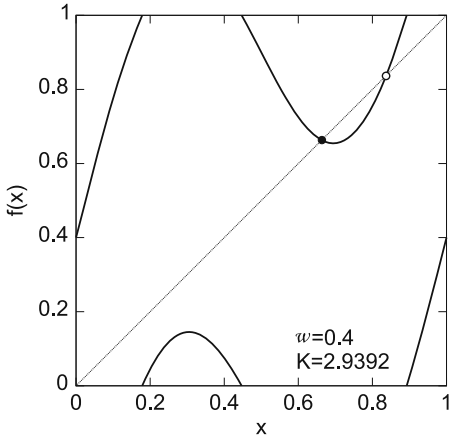

Fig. 7.13 The mapping function of the circle map. $f(x) = x + \omega + \frac{K}{2\pi} \sin 2\pi x \bmod 1$. $\omega = 0.4$, $K = 2.9392$. The *filled* and the *open circles* in the graph represent the stable and the unstable fixed points of the dynamics generated by this map

consider a network of circle-map units, defined as follows:

$$x_{n+1}^i = f(x_n^i + c \sum_{i \neq j} w_n^{ij} x_n^j) \tag{7.13}$$

where f is the mapping function of circle map, i.e., $f(x) = x + \omega + \frac{K}{2\pi} \sin 2\pi x \bmod 1$ and c represents the strength of the interaction between units as in the previous model. The dynamics of connection weights w_n^{ij} are the same as in the previous model (Eq. (7.3)).

Besides showing synchronization/desynchronization and clustering as in the previous model, this model exhibits a novel kind of collective dynamics, i.e. synchronized intermittent bursting. In this section, we focus on the structure formation related to this type of dynamics; parameter values are set to $(\omega, k, c, \delta) = (0.4, 2.9392, 0.1, 0.01)$. The initial conditions in simulations are same as in the previous section: uniform, all-to-all coupling and random state variables.

7.3.2 Unit Dynamics

As mentioned above, our model shows synchronized bursting for the parameter values we use here. Figure 7.14 (top) shows the temporal evolution of state variables around the beginning of a simulation. For most of the time, units stay near the stable fixed point, the value of which is represented by the brightest color in the gray scale. From time to time, units simultaneously show excursions from the fixed point, indicated by the simultaneous appearance of darker colors for all the units. This excursion does not last so long: most of the units return to the position near the fixed point within a few steps.

We refer to the state where most of the units stay around the fixed point as the resting state, and the state where most of the units show excursion dynamics as the bursting state. The transition between the resting and bursting states is captured by computing the dynamics of the mean of the state variables, or the mean field X_n defined as $X_n = \frac{1}{N} \sum_i x_n^i$. The time series of the mean field corresponding to the unit dynamics shown in Fig. 7.14 (top) is plotted in Fig. 7.14 (bottom). The resting state is represented by periods of almost constant mean field, while the bursting state is characterized by fluctuating mean field dynamics with a large amplitude.

This amplitude gets smaller as simulation time elapses. Figure 7.15a is the time series of the mean field during 37,000–38,000 steps. The resting and bursting states cannot be clearly distinguished as in the early stage. This seems to indicate that the bursts of units get less synchronized. However, although system-wide synchronized bursting no longer exists, synchrony within subgroups of units is still preserved. Figure 7.15b–d are the mean fields of three subgroups of units. Transition between the resting and bursting states can be observed in these mean fields, indicating synchronous bursting of units within each of the subgroups. These subgroups show

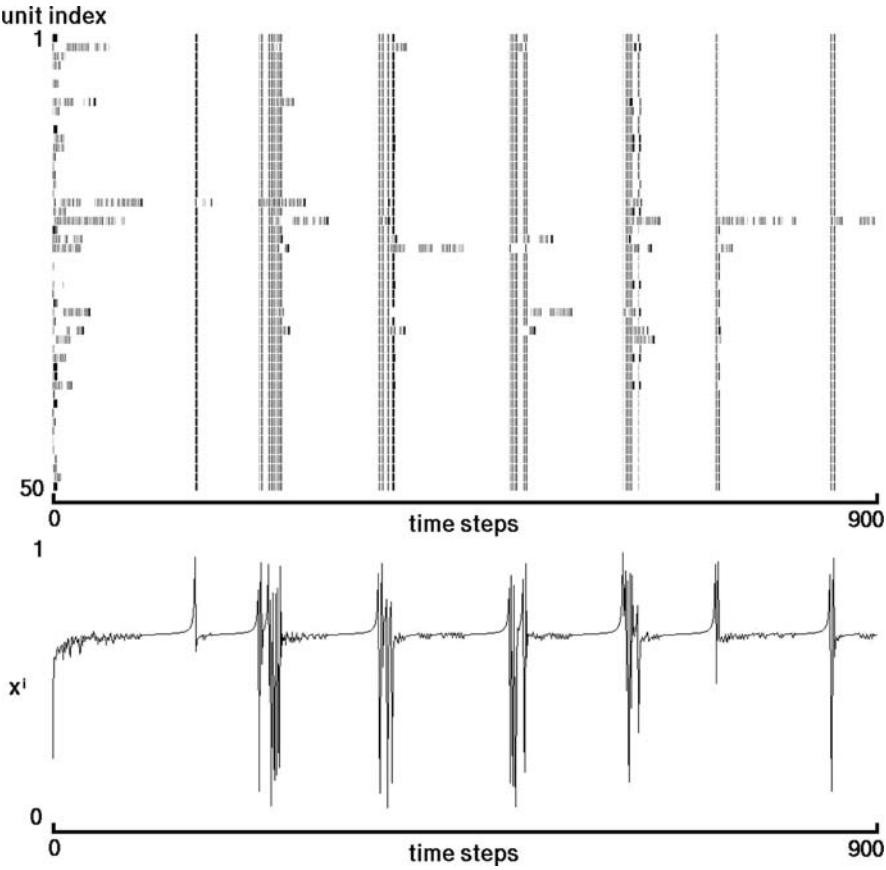

Fig. 7.14 Synchronized intermittent bursting of units in the model of coupled circle maps, observed at the beginning of a simulation. (*top*) Time series of the state variables x_n^i. Values of x_n^i are plotted in a gray scale, where the brightest color is assigned to the stable fixed point of unit dynamics. The color gets darker as x_n^i takes more distant values from the fixed point. (*bottom*) Time series of the corresponding mean field

bursting with different timings, which leads to the diminished fluctuation in the grand mean field shown in Fig. 7.15a. Such separation of units into synchronizing subgroups is achieved via the interaction between unit and connection dynamics. Indeed, the synchronized subgroups can easily be identified by looking at the connection matrix.

7.3.3 Connection Dynamics

Figure 7.16 is the connection matrix at the 37,000-th step of the simulation shown in Fig. 7.15. Units are clearly partitioned into three groups, each of which having

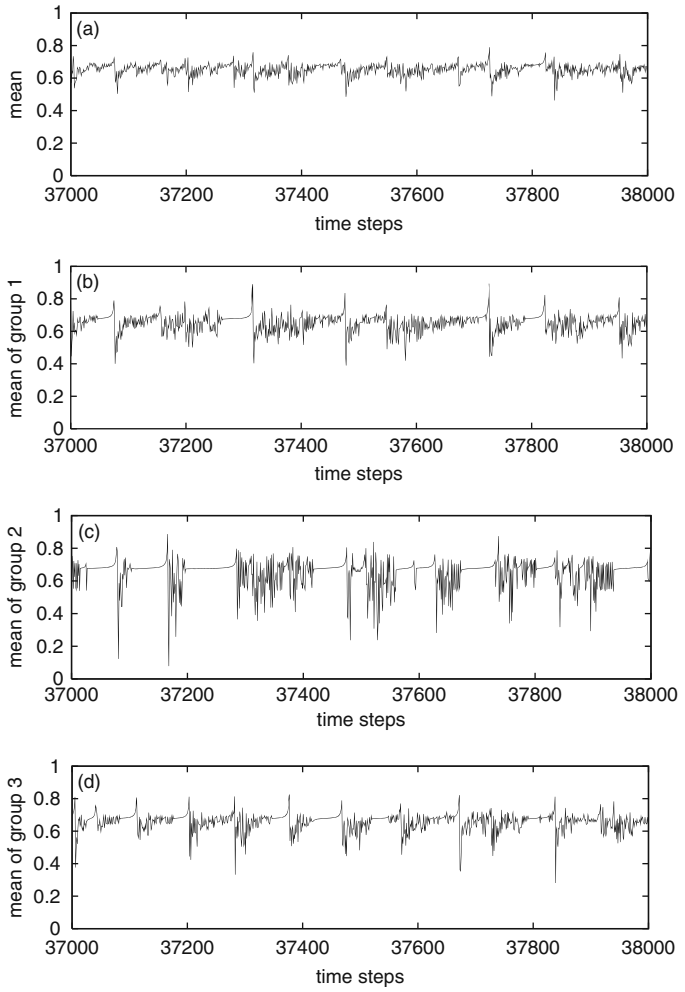

Fig. 7.15 Time series of the mean field, observed after 37,000 steps of temporal evolution. (**a**) The mean field of the whole system. (**b–d**) The mean fields of three subgroups in the system. These subgroups are identified from the connection matrix shown in Fig. 7.16. The groups shown in (**b**), (**c**) and (**d**) are the ones driven by the pacemakers 1, 2 and 3 shown in Fig. 7.16, respectively

a single unit with massive outgoing connections. We call such units pacemakers, because the synchronized bursting of the units within a group is achieved in the form that the group's pacemaker drives the other units to burst. Note that the synchronized bursting in the early time steps is mediated by uniform, all-to-all connection, meaning that the mechanism of the synchronized bursting is different in the early and the later stage of temporal evolution.

To illustrate the process of the formation of pacemakers, we plot the time series of $W_{\text{out}}{}^{i}$ values in Fig. 7.17. As mentioned above, there is no pacemaker at the

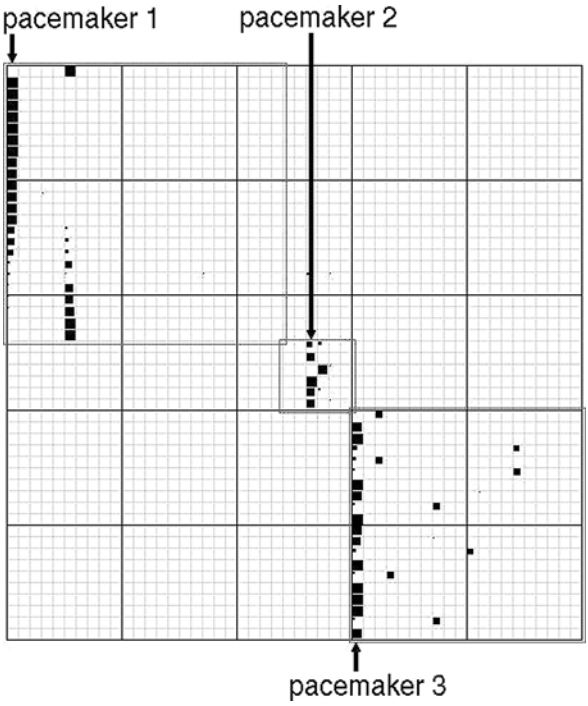

Fig. 7.16 Connection matrix at the 37,000th step of the simulation trial shown in Fig. 7.15. Pacemakers are indicated by the *arrows*. The range of the units driven by each of the pacemakers are indicated by the *square*. Note that, in the group of pacemaker 1, a new pacemaker (the 6th unit) which is still mutually coupled with pacemaker 1 is being formed

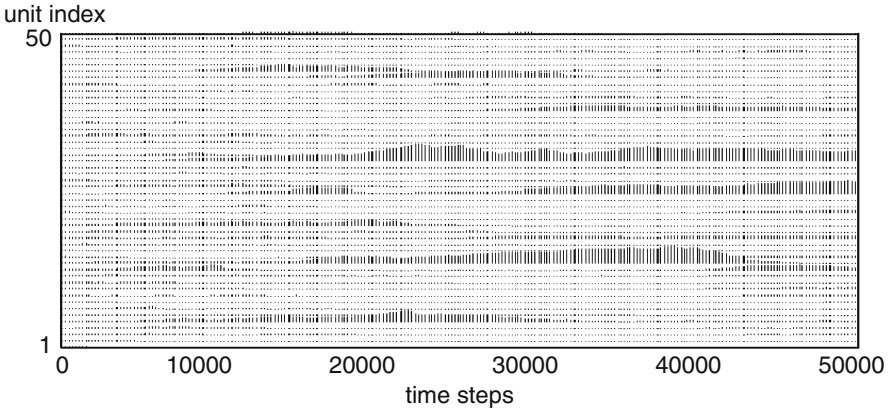

Fig. 7.17 Time series of $W_{\text{out}}{}^{i}$. The length of vertical tics represent the values of $W_{\text{out}}{}^{i}$. This is the same simulation trial as shown in Fig. 7.15

beginning of the simulation. As time elapses, the distribution of $W_{\text{out}}{}^{i}$ values starts to show a bias. By the 20,000th step of the simulation shown in Fig. 7.17, a few units have gained extremely large $W_{\text{out}}{}^{i}$ values compared to the others. These units work as the pacemakers. The separation of units into pacemakers and the rest is not stable over time. Indeed, births and deaths of pacemakers can be seen in Fig.7.17, and this process is accompanied by the reorganization of the groups of synchronously bursting units.

7.3.4 Mechanism of Structure Formation

In this model, the formation of network structure is closely related to the transition between the resting and the bursting states. Noting that connection change hardly occurs during the resting state, where all the state variables take similar values, we can focus our attention on the connection change during the bursting state. As seen in Fig. 7.14, the onset of bursts is highly synchronized among units in the early time steps. However, the timing of the burst offsets is quite diverse among units: some units take much longer time steps to return to the resting state. It is highly likely that such units rapidly lose their outgoing connection weights to most of the other units, which are already in the resting state and whose state variables have quite similar values. This can be stated in the opposite way: the units that return to the resting state earlier than the other units are likely to grow their outgoing connection weights.

Based on this consideration, the mechanism of structure formation in this model can be summarized as follows. At the beginning, all units have the same amount of outgoing connection weights. Through the temporal evolution, more and more units lose their outgoing connection weight by failing to return quickly to the resting state after each burst. This process leads to the concentration of outgoing connection weights to a small fraction of units. Such units work as pacemakers and drive the other units to burst synchronously. Once a group of synchronously bursting units is formed, the connection between the units in different groups is weakened, because they burst with different timings. Thus, groups are separated and gain a certain degree of stability.

7.4 Formation of Hierarchical Network Structure Triggered by External Input

So far, we have considered the models composed of identical units and studied how heterogeneous network structure emerges from the homogeneous condition. However, it would also be of general interest to study how externally induced heterogeneity influences the formation of network structure. Here we briefly review the study of a model where the application of external input to a part of the system triggers the self-organization of a nontrivial network structure [18].

The model is formulated as follows:

$$x_{n+1}^{i} = x_n^i + \omega + \frac{K}{2\pi}\sin 2\pi x_n^i + \frac{c}{2\pi}\sum_j w_n^{ij}\sin 2\pi x_n^j + I^i, \tag{7.14}$$

where I^i is the external input to unit i. This model is essentially same as the one in the previous section, except for the slight difference in the manner of coupling. The dynamics of connection weights w_n^{ij} are same as in the previous models (Eq. (7.3)).

For appropriate sets of parameter values (for example, (ω, K, c, δ)=(0,4.1,1.0,0.1), which is used in the simulations shown below) in the desynchronized phase, this system shows self-organization into a nontrivial network structure upon the application of a constant external input to an arbitrary unit in the system. In this study, network structure is examined after mapping the network to a graph using digitization of connections, i.e. considering only the connections having a large weight, namely larger than 1.0, and ignoring weak ones. In order to examine the network structure using the obtained graph, a proper measure that extracts a salient network structure is necessary. By examining the connection matrix, we found that the generated network structure is characterized by "layers" of nodes. Layers in the network are defined as follows: first, we define the root node, which is the only node that belongs to the first layer, and then, define the subsequent layers as the group of the units that receives direct link from a unit in the previous layer.

In Fig. 7.18, the graph of the network generated under the application of an external input to a single unit (unit 00 in the figure) is illustrated by using this digitization,

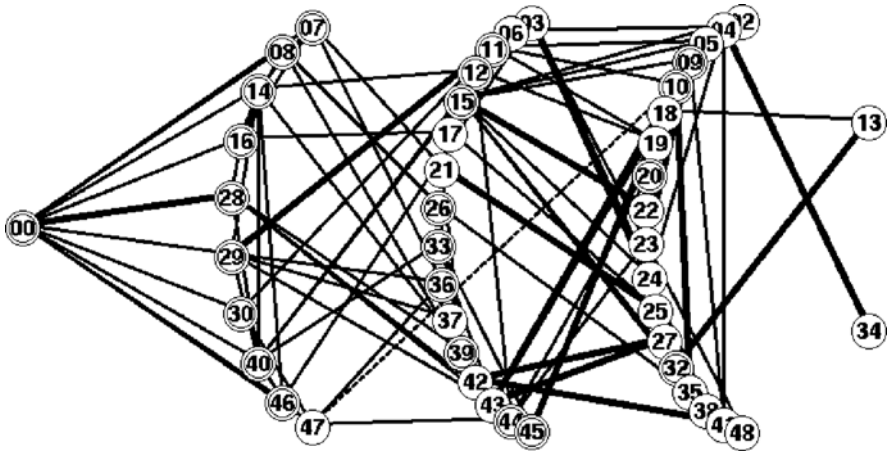

Fig. 7.18 The graph obtained from the connection matrix by digitalizing connections with a certain threshold. *Circles* represent units and the numbers inside are the unit IDs. Only unit 00 is supplied with external input, and this unit is the only constituent of the 1st layer. The arc of the units next to unit 00 is the 2nd layer, and the arc next to it is the 3rd layer, ... and so forth. The lines between *circles* are the links of the graph. *Thin lines* are the links directed from left to right and *thick lines* are bidirectional links. *Dashed lines* represent NLSC, i.e., the links between distant layers

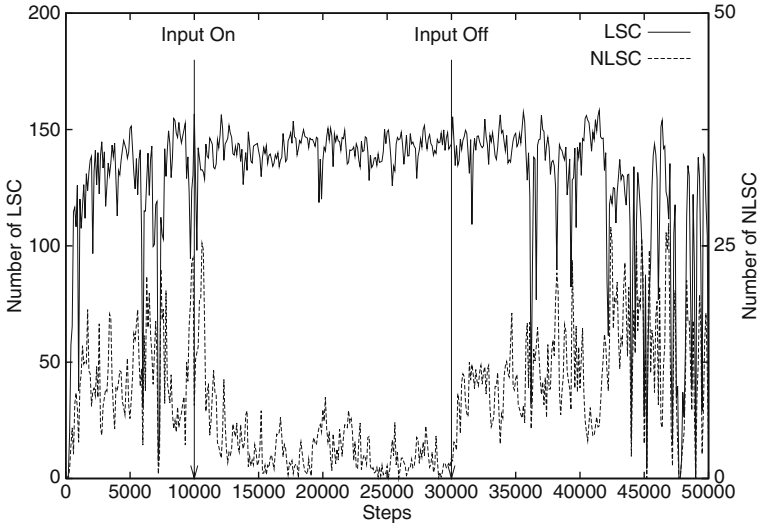

Fig. 7.19 Time series of the numbers of LSC and NLSC. The onset and the offset of external input are indicated by the arrows in the graph. See the main text for the definitions of LSC and NLSC

where layers are organized with the input unit at the root. Five layers are recognized in this case. A surprising finding about the networks self-organized in this model is that the most of connections are between neighbouring layers or within a layer, and that only little fraction of connections are between distant layers. Indeed, in Fig. 7.18, all the connections but one, which is drawn with dashed line, are between neighbouring layers or within a layer.

Here, we denote the connections between neighbouring layer or within a layer as layer structural connections (LSC) and the connections between distant layers as non-layer structural connections (NLSC). In Fig. 7.19, the numbers of LSC and NLSC are plotted in time. Note that the external input is applied only between 10,000th and 30,000th steps. After the application of input at 10,000th step, the number of NLSC shows a substantial decrease. Moreover, immediately after the cut-off of the input, the number of NLSC recovers to the same level as before the application of the input. This result clearly shows that the formation of the layered structure is dependent on the application of external input.

Some interesting dynamical properties such as a power law distribution of the lifetime of unit in a layer have been observed in this model, but the mechanism for this type of structure formation has not yet been uncovered.

7.5 Summary and Discussion

To summarize, we have introduced three types of coupled map models in order to study the self-organization of network structure in adaptive networks. First we

have shown the result of a coupled logistic-map system with Hebbian connection dynamics. In this system, we found spontaneous separation of units into two groups, one consisting of units with strong outgoing connections and the other consisting of units with weak outgoing connections. Only a small fraction of units belongs to the former group, and the rest of the units belonging to the latter are just driven by the dynamics of the former. Thus, the units with strong outgoing connections have more influence on the dynamics of the other units. In this sense, the emergence of a group of units with strong outgoing connections can be interpreted as the emergence of leadership in a population.

A similar self-organized network structure was observed in the second type of model, i.e., a coupled circle-map system. In this model, units self-organize into some synchronously bursting groups, and each group has a pacemaker unit which has strong outgoing connections and drives the dynamics of the other units. Though this model shows quite different unit dynamics from the logistic map model, its self-organized network structure is similar to that of the logistic map model in the point that only a small fraction of units attain the influential positions. This suggests that the emergence of leadership may be a general phenomenon in some class of adaptive networks.

It should be stressed that in these models all units are identical and the initial network structure is uniform, all-to-all connection. This means that the leaders emerge spontaneously from a homogeneous population, without any individual differences among units. In the third model, where external input is applied to only one unit in the system, units are not homogeneous. The self-organized structure in this system is more complex than in the other models: units self-organize into a hierarchical structure, where the unit with external input is located at the root and the other unit form several layers with decreasing centricity from the root node. There is a rule in the connectivity between the units in different layers, i.e. connections between distant layers are avoided. Thus, application of input to only one unit causes global reorganization of connection structure. This might be regarded as another example of the emergence of a leader which has strong influence on the behavior of the whole system.

We studied the mechanism of structure formation for the first model in detail, and extracted the steps of the process. First, variability among units is created by unit dynamics (the variability in the TGH interval is created by the chaotic dynamics). Then, in the next step, this variability is imprinted in connection weights (there is a simple relationship between TGH interval and the average correlation of units, which is directly reflected in the connection change). Finally, the connection structure influences the unit dynamics (we confirmed that units with strong outgoing connections have long TGH interval, resulting in the amplification of the variability in TGH interval). Thus, a closed loop of the interaction between unit dynamics and connection changes is formed. This results in a stable growth of network structure.

Such a feedback process is not properly at work in the second model, which might be the reason for the weaker stability of the structure in this model. There, the timing of returning to the resting state after bursts is distributed, and this variation is reflected in the outgoing connection strength. Up to here, the process is quite

similar to that in the first model. However, the last step is missing in the second model, and hence the feedback loop is not closed. If there were a process that makes pacemakers return quickly to the resting state, the network structure in this model should be stable. Instead, this model has a process such that a stronger outgoing connection enhances the burst synchrony within a group, which only weakens the connections between units in different groups.

We expect that the mechanism of the structure formation we have found here is rather general in adaptive networks with mutual feedback between chaotic dynamics and coupling with Hebbian-type dynamics. These three steps for the structure formation clarified above will be discovered in other class of models of adaptive networks where the emergence of leadership (or strong heterogeneity) is observed, or, conversely, it will be possible to design a system to form leaders spontaneously from a homogeneous population by implementing these three steps in the system's dynamics.

Acknowledgements The authors thank Dr. Abigail Morrison for her careful reading of the manuscript.

References

1. R. Albert and A. -L. Barabási, Rev. Mod. Phys. **74**, 47 (2002).
2. S. N. Dorogovtsev and J. F. F. Mendes, *Evolution of Networks* (Oxford University Press, Oxford, 2003).
3. M. E. J. Newman, A. -L. Barabási and D. J. Watts, *The structure and dynamics of networks* (Princeton University Press, Princeton, 2006).
4. A. -L. Barabási and R. Albert, Science **286**, 509 (1999).
5. D. J. Watts, *Small World* (Princeton University Press, Princeton, 1999).
6. E. Almaas, B. Kovács, T. Vicsek, Z. N. Oltvai and A.-L. Barabási, Nature **427**, 839 (2004).
7. C. Furusawa and K. Kaneko, Phys. Rev. E **73**, 011912 (2006).
8. M. Barahona and L. M. Pecora, Phys. Rev. Lett. **89** 054101 (2002).
9. T. Nishikawa, A. E. Motter, Y. C. Lai, and F. C. Hoppensteadt, Phys. Rev. Lett. **91**, 014101 (2003).
10. H. Kori and A. S. Mikhailov, Phys. Rev. E **74**, 066115 (2006).
11. S. C. Manrubia and A. S. Mikhailov, Phys. Rev. E **60**, 1579 (1999).
12. J. Jost and M. P. Joy, Phys. Rev. E **65**, 016201 (2002).
13. W. L. Lu, F. M. Atay and J. Jost, Eur. Phys. J. B (2008) doi: 10.1140/epjb/e2008-00023-3.
14. F. H. Willeboordse Phys. Rev. Lett. **96**, 018702 (2006).
15. R. E. Amritkar and S. Jalan, Physica A **321**, 220 (2003).
16. J. Ito and K. Kaneko, Phys. Rev. Lett. **88**, 028701 (2002).
17. J. Ito and K. Kaneko, Phys. Rev. E **67**, 046226 (2003).
18. J. Ito and K. Kaneko, Neural Netw. **13**, 275 (2000).
19. J. Ito and T. Ohira, Phys. Rev. E **64**, 066205 (2001).
20. P. Gong and C. van Leeuwen, Europhys. Lett. **67**, 328 (2004).
21. C. S. Zhou and J. Kurths, Phys. Rev. Lett. **96**, 164102 (2006).
22. T. Gross and B Blasius, J. R. Soc. Interface **5**, 259 (2008).

23. K. Kaneko, Prog. Theor. Phys. **72**, 480 (1984).
24. K. Kaneko, Physica D **34**, 1 (1989).
25. K. Kaneko, Physica D **41**, 137 (1990).
26. K. Kaneko and I. Tsuda, *Complex Systems: Chaos and Beyond* (Springer, Berlin, 2000).
27. K. Kaneko, Physica D **75**, 55 (1994).